CrossMark

Large pyroelectric properties at reduced depolarization temperature in A-site nonstoichiometry composition of lead-free $0.94Na_xBi_yTiO_3$–$0.06Ba_zTiO_3$ ceramics

A. M. Balakt[1], C. P. Shaw[1], and Qi Zhang[1,*]

[1] School of Aerospace, Transport and Manufacturing, Cranfield University, Cranfield, Bedfordshire MK43 0AL, UK

ABSTRACT

Nonstoichiometry lead-free $0.94Na_xBi_yTiO_3$–$0.06Ba_zTiO_3$ (N_xB_yT–$0.06B_zT$) (from $x = y = 0.5$, $z = 1.00$ to $x = 0.5$, $y = 0.534$, $z = 1.02$) ceramic compositions were prepared by a conventional solid-state route. XRD shows that the compositions are at a morphotropic phase boundary where rhombohedral and tetragonal phases coexist. The depolarization temperature (T_d) can be lowered by modifying x, y and z. The pyroelectric coefficient (p) of nonstoichiometry N_xB_yT–$0.06B_zT$ compositions is greatly increased, compared with stoichiometry NBT–0.06BT composition, from 3.15×10^{-4} C m^{-2} °C^{-1} at room temperature (RT) and 23.9×10^{-4} C m^{-2} °C^{-1} at T_d, and reaches maxima of 6.99×10^{-4} C m^{-2} °C^{-1} at RT and 75.3×10^{-4} C m^{-2} °C^{-1} at T_d for $x = y = 0.52$ and $z = 1$. The figures of merits, F_i, F_v, and F_D, also have been improved from 1.12×10^{-10} m v^{-1} and 0.021 m^2 C^{-1} to 2.50×10^{-10} m v^{-1}, 0.047 m^2 C^{-1} and 16.63×10^{-6} Pa$^{-1/2}$, respectively, for $N_{0.52}B_{0.52}T$–0.06BT composition at RT. Furthermore, $N_{0.52}B_{0.52}T$–0.06BT composition shows a huge enhancement in F_i, F_v and F_D to 26.9×10^{-10} m v^{-1}, 0.39×10^{-10} m^2 C^{-1} and 138.7×10^{-6} Pa$^{-1/2}$, respectively, at T_d. The same composition also presents F_C values which are ~ 2.58 and ~ 2.86 ($\times 10^{-9}$ C cm^{-2} °C^{-1}) at RT at 100 and 1000 (Hz). $N_{0.5}B_{0.534}T$–0.06BT and $N_{0.5}B_{0.534}T$–$0.06B_{1.02}T$ compositions show a large p values at a wide temperature range. The enhanced pyroelectric properties make nonstoichiometry $N_{0.52}B_{0.52}T$–0.06BT composition a promising candidate for pyroelectric and other applications at wide temperatures range.

Introduction

Pyroelectric ceramic materials have been used as an active element in various electronic devices [1, 2]. These materials are playing a major role in diverse applications such as sensors, infrared detectors, thermal cameras, remote medical diagnostic devices, gas detectors, and many other applications. PZT-based multicomponent ceramic materials are the most widely utilized in electronic applications due to

Address correspondence to E-mail: q.zhang@cranfield.ac.uk

their superior ferroelectric, pyroelectric, and piezo-electric properties, but environmental issues relating to the hazardous nature of lead-containing materials and its disposal are driving the need to find lead-free ceramic materials as an alternative to fill the industrial gap [1–3].

Lead zirconate titanate (PZT) and PZT-based materials exhibit exceptional ferroelectric properties around the morphotropic phase boundary (MPB). Consequently, effort has focused on alternative lead-free materials that possess an MPB region as replacements for PZT-based materials, and such materials have been explored in the past few decades [2]. $(1 - x)(Na_{0.5}Bi_{0.5})TiO_3–xBaTiO_3$ (NBT–xBT) as a lead-free system has attracted interest of numerous researchers due to its high ferroelectric properties at the MPB at $x = 0.06$–0.07 [1, 2, 4, 5], and the lower coercive field here which makes poling easier [5]. The phase diagram of NBT–0.06BT is complex and presents many phases. Firstly, from ferroelectric (FE) to antiferroelectric (AFE) or to relaxor at depolarization temperature (T_d), it is reported at around 100 to ∼165 °C [6–13]. Secondly, from antiferroelectric (AFE) to nonpolar (PE) phases, it happens at around 225–292 °C, at either Curie temperature (T_c) or the temperature at the maximum dielectric permittivity (T_m) [6–10, 12]. The NBT–0.06BT phase transitions are also associated with structural changes, which can be either from rhombohedral (Rh) and tetragonal (Tr), if the composition is at the MPB, or from rhombohedral (Rh), if the composition is out of MPB, to tetragonal (Tr), and from tetragonal (Tr) to cubic (C) [9, 11, 12]. These structural phase changes are very important to the pyroelectric applications because large pyroelectric effects can be induced at these transitions.

NBT–0.06BT has been extensively investigated for dielectric, ferroelectric, and piezoelectric properties but to a lesser extent in terms of its pyroelectric properties [7, 9, 14, 15]. In previous work, we investigated the effects of Ba^{2+} content on the pyroelectric properties of NBT–0.06B$_{(1+x)}$T ceramics [2] and found that p increased from 2.90 to 3.54 ($\times 10^{-4}$ C m^{-2} C^{-1}) at RT when $x = 1.02$. In addition, p showed huge enhancement from 55.3 to 740.7 ($\times 10^{-4}$ C m^{-2} C^{-1}) at T_d (85 °C) for the composition NBT–0.06B$_{1.02}$TiO$_3$ [16]. Follow on studies on this work, reported the effects of Ta doping in NBT–0.06BT with the pyroelectric coefficient highly enhanced from 3.14 to 7.14 ($\times 10^{-4}$ C m^{-2} C^{-1}) at RT at Ta = 0.2% with the same composition showing a maximum value of

146.10 $\times 10^{-4}$ C m^{-2} C^{-1} at T_d (78.8 °C) [16]. Furthermore, our recent investigation of NBT–0.06BT doped with La reveals that the pyroelectric properties of NBT–0.06BT were greatly improved by La doping from 3.14 to 7.42 ($\times 10^{-4}$ C m^{-2} °C^{-1}) at RT at La = 0.5% and to 105.40 $\times 10^{-4}$ C m^{-2} °C^{-1} at T_d (67.9 °C) at La = 0.2% [17].

Pyroelectric properties usually reach a peak value at phase transition temperatures, such as T_d and T_c. These two phase transition temperatures in NBT–0.06BT are far too high for practical use at room temperature, so it would be beneficial if these phase transition temperatures can be lowered. In this study, we expect to bring down the depolarization temperature by modifying the stoichiometric state of the compositional contents x, y, and z of NBT–0.06BT, to simultaneously improve the pyroelectric properties of these compositions at both RT and T_d.

Experimental

A solid-state synthesis technique was selected to prepare the stoichiometry 0.94NBT–0.06BT (NBT–0.06BT) and nonstoichiometry $0.94Na_xBi_yTiO_3–0.06Ba_zTiO_3$ (Na$_x$Bi$_y$T–0.06Ba$_z$T) compositions. The reagents used in this project were bismuth oxide (Bi$_2$O$_3$), 99.999%, sodium carbonate (Na$_2$CO$_3$), 99.5%, barium carbonate (BaCO$_3$), 99.98%, and titanium dioxide (TiO$_2$), >99.8% (all Sigma-Aldrich).

The amounts of powders were calculated according to the chemical formula of $0.94Na_xBi_yTiO_3–0.06Ba_zTiO_3$, with the x, y, and z values for each composition listed in Table 1, where the start composition of B is modified by receive an extra 0.02 from Na(x) and Bi(y) concentrations and the composition of C is also changed by modify the y/x ratio to be >1, while the start composition of D is as same as composition C with extra Ba (z) 0.02 concentration, as given in Table 1. The raw materials were ball-milled (zirconia milling media) in acetone in polyethylene pots for 24 h in order to mix and mill the powders. The resultant slurries were dried overnight at 50 °C, and the dried powder cakes were ground in a mortar for 10 min and sieved through a 250-μm mesh in order to aid the calcination step. The powders were calcined at 850 °C for 180 min in a closed alumina crucible with a heating ramp rate of 1 °C per minute and cooling rate 5 °C per minute in a furnace (Pyro Therm, ITEMP 14/6). After calcination, the powders

Table 1 Lattice parameters (Å), cell volume (Å³), tolerance factor, grain size, and density (gm cm^{-3}) of NBT–0.06BT and N$_x$B$_y$T–0.06B$_z$T ceramics

Composition, name	Lattice parameter (Å)		c/a ratio	Average grain size (μm)	Density (ρ) (gm cm^{-3})
	a	c			
NBT–0.06BT, A	5.5113	13.4744	2.4449	1.79	5.757
N$_{0.52}$B$_{0.52}$T–0.06BT, B	5.4914	13.5048	2.4595	1.67	5.754
N$_{0.5}$B$_{0.534}$T–0.06BT, C	5.5113	13.4902	2.4516	1.55	5.541
N$_{0.5}$B$_{0.534}$T–0.06B$_{1.02}$T, D	5.4957	13.5048	2.4586	1.41	5.704

were re-milled in acetone for 24 h, and then, 2% (wt.) of poly vinyl alcohol (PVA) was added as an organic binder to the dried powders to enhance the mechanical strength of the pellets during pressing. After that, the powders were fully dried in oven at 80 °C. The dried powders were ground and sieved and subsequently pressed into green pellets with a diameter of 10 mm under an uniaxial compaction with a load of ~78MPs for 5 min at RT. The pellets were sintered at temperatures up to 1150 °C for 120 min in closed crucibles in order to minimize the loss of volatile Na$^+$ and Bi^{3+}. The pellets were lapped/polished on both sides using silicon carbide paper. Silver conductive paint (RS limited) was used to electrode the pellets, and electrical poling at 6.5 kV/mm for 10 min at RT in mineral oil was carried out using a Keithley (6517 electrometer/high resistance) DC power supply. Afterwards, the poled samples were washed thoroughly by using isopropanol in order to remove the mineral oil and then left in air for 3 h to dry. The poled samples were placed at RT for 60 min with their electrodes short-circuited to eliminate any unwanted trapped charges.

SEM (FEI XL30 SFEG) was used to look at the grain morphology of the sintered samples, and X-ray diffraction (XRD) [Siemens Ltd Model: D500] was used to investigate crystallization and phase. Dielectric measurements were performed on an impedance analyser (Wayne kerr Electronics Ltd. Model 3245 and Hewlett Packard HP4092A)] over a temperature range from RT to 150 °C using a custom-built temperature-controlled hotplate in the frequency range of 0.1–10 kHz. Pyroelectric measurements were made using the Byer–Roundy [18] method on a custom-built computer-controlled rig which used thermoelectric heaters to ramp the temperature between 20 and 90 °C while under vacuum and collect the pyroelectric current response from a Keithley electrometer (Model 6217). Dielectric and pyroelectric data were then used to study the phase changes such as depolarization temperatures (T_d) and to determine figure of merit values F_i, F_v, F_D, and F_C.

Results and discussion

Effects of nonstoichiometry composition on microstructure

Figure 1a depicts the XRD spectra of stoichiometry and nonstoichiometry ceramic powders calcined at 850 °C for 3 h. All the compositions present a single-crystalline perovskite structure with no evidence of any secondary phases indicating that the excess Na$^+$, Bi^{3+}, and Ba^{2+} diffused into the NBT–0.06BT main lattice and formed the new nonstoichiometry N$_x$B$_y$T–0.06B$_z$T ceramic solid solutions [19, 20].

Figure 1b illustrates a splitting of the peak [111] into [003] and [021] at 39.0°–41.0°, for all the compositions showing the existence of the rhombohedral (Rh) phase. This split coincides with that observed in the X-ray diffraction spectra of the unmodified or undoped NBT [11, 19].

A similar splitting was identified in all compositions for the [200] peak into [200] and [002] at 46.0°–48.0° as shown in Fig. 1c, which indicates the presence of tetragonal (Tr) phase in the N$_x$B$_y$T–0.06B$_z$T lattice [11, 20, 21]. The coexistence of both Rh and Tr phases in the N$_x$B$_y$T–0.06B$_z$T ceramics confirms that the structures of stoichiometry composition (A) are at the MPB and also the nonstoichiometry compositions (B, C, and D) remain at MPB area. Although the stoichiometric state of B, C, and D has been changed by modifying the elements molar concentrations (x, y, and z) in this study as mention before, XRD patterns show no significant changes in the phase structure of nonstoichiometry N$_x$B$_y$T–0.06B$_z$T compositions compared with the stoichiometry composition which is in agreement with the literature [11, 19, 21, 22].

Figure 1 **a** XRD patterns of NBT–0.06BT and N_xB_yT-$0.06B_zT$; **b** enlargement of [111] peak split into [003] and [021] at 39.0°–41.0°; and **c** enlargement of [200] peak split into [200] and [002] at 46.0°–48.0°.
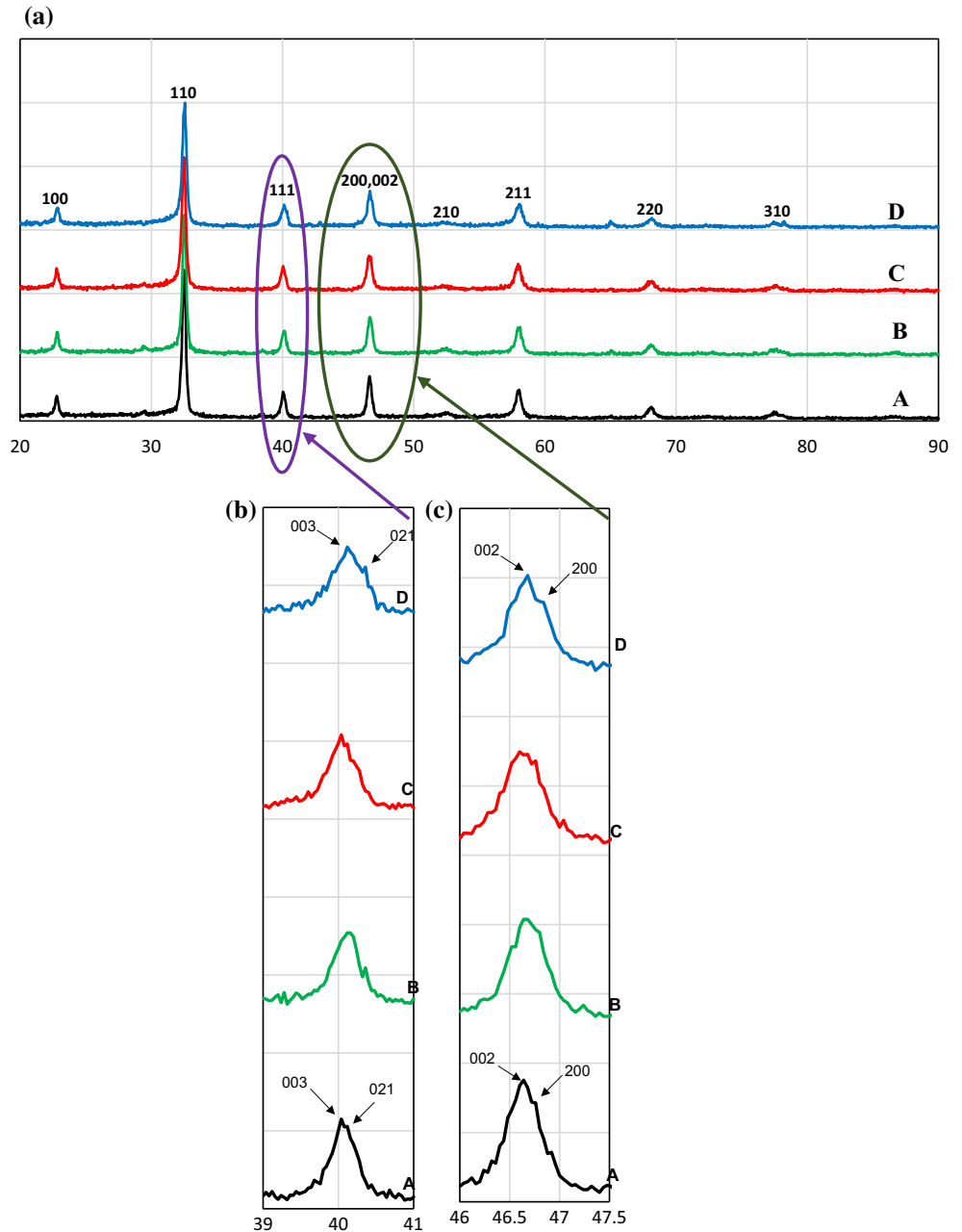
According to the ionic matching relationship [23], the ionic radius of all elements in the compositions is Na^+ (1.39 Å, CN 12) (CN = coordination number), Bi^{3+} (1.31 Å, CN 12), Ba^{2+} (1.61 Å, CN12), and for Ti^{4+} (0.61 Å, CN 6). The excess in the elements content will compensate the loss of elements due to evaporation at the calcining and sintering stages and may also substitute other cations in the composition [24]. For instance, the excess in the barium content in Composition D may compensate the deficiency in the Ba^{2+}, which will improve the tetragonality in the $N_{0.5}B_{0.534}TiO_3$–$0.06B_{1.02}T$ composition [2], simultaneously being more likely to substitute the sodium than replace the bismuth in NBT due to the larger radial difference (>15% for Bi) [19].

To determine the stability of the perovskite structure, Goldschmidt tolerance factor (*t*) relation was calculated by using Eq. 1 [25–28]:

$$t = \frac{R_A + R_O}{\sqrt{2}(R_B + R_O)} \tag{1}$$

where R_A, R_B, and R_o are the ionic radius of ions which will occupy A, B sites, and the oxygen anion. The tolerance factor value of stable perovskite structure is in the range of 0.77–0.99 [27]. The average t value which has been calculated for the stoichiometry and nonstoichiometry compositions in this study is around 0.982, suggesting that all compositions illustrate stable structure.

Table 1 illustrates the lattice parameters (Å), the c/a ratio, the average grains size (μm), and samples density (g cm^{-3}) of all compositions. The lattice parameters are "$a = b$" and "c" vary by modifying x, y, and z contents. The c parameter shows a slight increase from composition A to D. Compositions B, C, and D have higher c/a ratio than Composition A indicating that the nonstoichiometry Compositions B, C, and D have more tetragonality in their structure. This result is in agreement with the Yoon et al. [29] results.

Figure 2 shows the SEM surface morphology of the Compositions A, B, C, and D. All the compositions display a dense microstructure with an average density of around 5.689 ± 0.264 g cm^{-3}. Although B, C, and D have nonstoichiometry compositions with excess sodium, bismuth, and barium contents, they present a lower density value than Composition A (Table 1). Stoichiometry and nonstoichiometry compositions show a granule grain shape with various grain sizes. The average grain size reduces gradually from Compositions A to D (Table 1). The reason behind the reduction in the average grain size may link to the compositional changes that happened during calcining and sintering at high temperature. The loss of Na$^+$ is more likely higher than that of Bi^{3+} due to the larger volatility of Na$^+$. Thus, the composition may shift to a bismuth-nonstoichiometry state after calcining and sintering. Generally, the bismuth behaves as an inhibitor of the grain growth in the NBT structure. Hence, the excess in bismuth content in Composition B can reduce the grain size [11].

Both Compositions C and D are bismuth nonstoichiometric. Therefore, the effect of the Bi^{3+} on grain size is more pronounced in these compositions. Composition D presents the smallest grain size, which is due to the influence of Bi^{3+} and Ba^{2+} nonstoichiometric (excess content), and both of which may boost the prevention of the grain growth [2, 19, 29, 30]. In PZT ceramics, similar results (grain
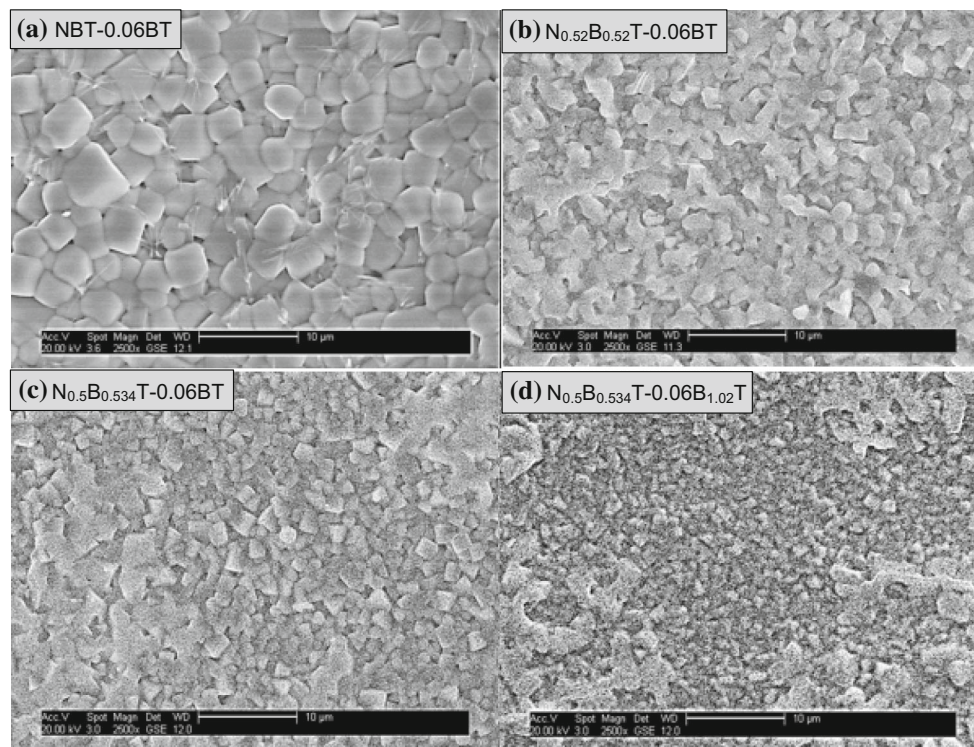

Figure 2 SEM surface morphology of NBT–0.06BT and N_xB_yT–$0.06B_zT$ ceramic compositions.

size reduction) have been reported where lead was substituted with barium [2, 19, 29, 30].

Effects of nonstoichiometry composition on dielectric properties

Modifying the stoichiometric state of the starting composition has a big effect on the magnitude of the dielectric properties of the $N_xB_yT–0.06B_zT$ material. Figure 3a–d presents the change of the dielectric properties of poled compositions from A to D as a function of temperature from 20 to 150 °C at 1, 10, and 100 (kHz). The relative permittivity (ε_r) of all the compositions increases with temperature, which behaves like a typical ferroelectric material [31].

The relative permittivity (ε_r) shows a significant increase with the increase in the x, y, and z contents,

with values of 396, 597, 893, and 933, respectively, for the Compositions A to D at RT and 1 kHz; therefore, the small variation in start compositions can be responsible for the significant increase in the relative permittivity value [24].

The dielectric loss ($\tan\delta$) also increases with the temperature up to a certain point and then decreases. The $\tan\delta$ value of Composition A is ~ 0.0436 at RT and 1 kHz (Fig. 3a). It increases for nonstoichiometry Compositions C and D to around 0.0531 and 0.0561, respectively (Fig. 3b–d). However, Composition B presents unexpected dielectric loss value (~ 0.0427) which is the lowest value among all other compositions (Fig. 3b).

The temperature at which $\tan\delta$ shows a maximum value is widely known as the depolarization
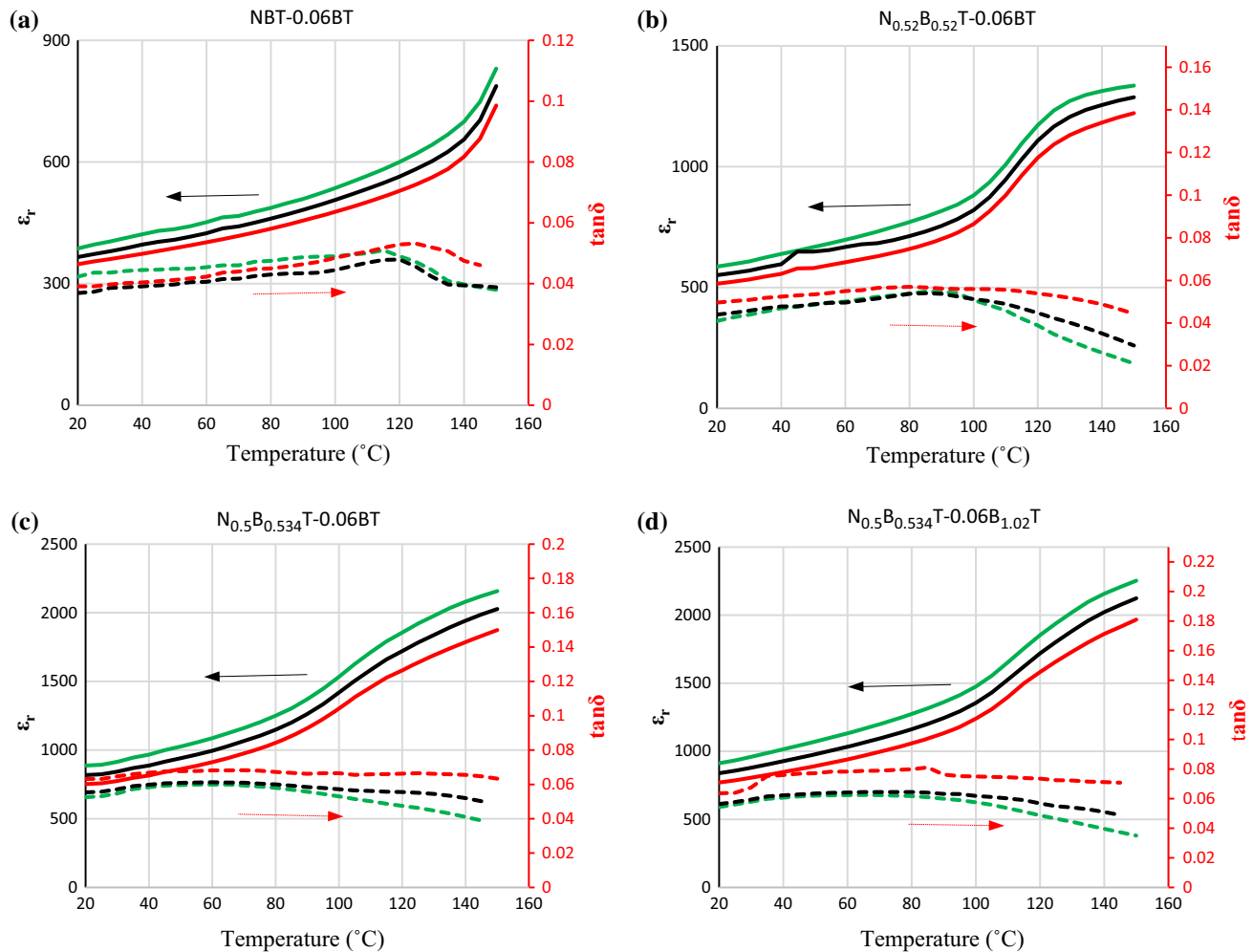

Figure 3 Relative permittivity (ε_r) and loss tangent ($\tan\delta$) versus temperature for **a** NBT–0.06BT, **b** $N_{0.52}B_{0.52}T$-0.06BT, **c** $N_{0.5}B_{0.534}T$–0.06BT, and **d** $N_{0.5}B_{0.534}T$–0.06$B_{1.02}T$ at three different frequencies 1, 10, and 100 (kHz), where *green dotted line* ε_r-1, *black dotted line* ε_r-10, *red dotted line* ε_r-100, *green solid line* $\tan\delta$-1, *black solid line* $\tan\delta$-10, *red solid line* $\tan\delta$-100.

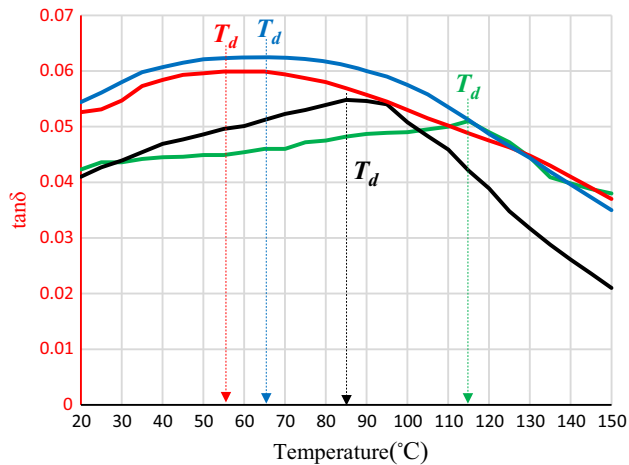**Figure 4** The identification of the T_d values of all compositions by dielectric method [loss tangent (*tanδ*) against temperature (°C)] for NBT–0.06BT and $N_xB_yT–0.06B_zT$ at 1 kHz, where *green solid line* Composition A, *black solid line* Composition B, *red solid line* Composition C, *blue solid line* Composition D.

Figure 5 Pyroelectric coefficient (*p*) versus temperature at different *x*, *y*, and *z* contents of NBT–0.06BT and $N_xB_yT–0.06B_zT$ ceramics, where *green solid line* Composition A, *black solid line* Composition B, *red solid line* Composition C, *blue solid line* Composition D.

temperature (T_d) [13, 32, 33]. The *tanδ* values at T_d are around 0.0510, 0.0548, 0.0599, and 0.0625, and their corresponding temperatures estimated at ∼115, 85, 55, and 65 (°C) for Compositions A, B, C, and D, respectively (Fig. 4). The *tanδ* results at T_d reveal that B shows the lowest value among all other compositions. The ε_r values at T_d are ∼582, 792, 1055, and 1105 for Compositions A, B, C, and D, respectively (Fig. 3a–d). The ε_r values at T_d clearly present that the change in the nonstoichiometric state of the composition has a significant effect on the dielectric properties, but the dramatic effect is on the relative permittivity at wide temperature range.

Effects of nonstoichiometry composition on depolarization temperature

Changing the stoichiometric state of the composition can also make a large effect on the depolarization temperature (T_d) of the $N_xB_yT–0.06B_zT$ compositions, where the $Na_{0.49}Bi_{0.50}TiO_3$ shows lower T_d than $Na_{0.50}Bi_{0.50}TiO_3$ [24]. Although depolarization temperature is an important parameter in pyroelectric study, its origin has not been fully understood for NBT–*x*BT. It has more than one definition [27, 32, 34–37], which includes the phase transition temperature from ferroelectric (FE) to antiferroelectric (AFE) phases or from ferroelectric to relaxor [33, 34, 38, 39].
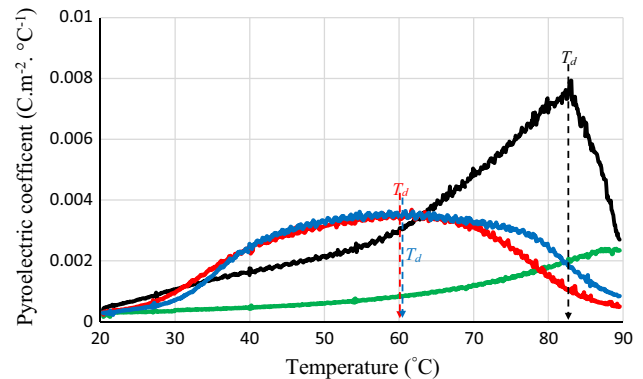
In this study, the T_d is subjectively identified by two methods: (1) dielectric method, from the dielectric loss peak value versus temperature plots (Fig. 4), and (2) pyroelectric method, the pyroelectric coefficient (*p*) peak value versus temperature plots (Fig. 5) [14]. For both methods, the T_d is strongly dependent on modifying *x*, *y*, and *z* concentrations of the compositions. Figure 4 reveals that T_d decreased from 115 °C in Composition A to around 55 °C for Composition C, respectively. Composition D illustrates a higher T_d, which is more than 10 °C higher than the T_d for Composition C (Fig. 4), whereas a shift to lower temperature for Ba^{2+}-nonstoichiometric composition was expected according to our previous study [2].

T_d can also be obtained from the maximum pyroelectric coefficient values. It is widely known that the maximum *p* can be achieved at the phase transition temperature [40–43]. In this study, T_d values identified by this method showed a decrease from more than 90 °C to ∼82.7, 60.0, and 60.6 °C for Compositions A to D, respectively. The exact T_d could not be identified for Composition A by the pyroelectric method due to the upper temperature limit of equipment (Fig. 5). In addition, Composition D shows a similar T_d to Composition C although as mentioned above, a lower value with increasing the Ba^{2+} content [2] was expected. The Bi^{3+} nonstoichiometric (excess content) in Composition D may be the reason for unexpected high T_d in both methods.

The decrease in T_d for nonstoichiometry compositions is probably caused by the excess amount of

bismuth and/or deficiency of sodium and also by extra barium concentration in the case of Composition D. According to Yoon et al. [29], Guo et al. [33], and Li et al. [44], the T_d coincides with phase transition from ferroelectric to a so-called intermediate phase phase, and this transition shows a shift of T_d towards lower temperature for compositions with excess Bi^{3+} and/or deficit of Na^+. Excess Bi^{3+} concentration in the Compositions B, C, and D is more likely to replace the A-site ions, Na^+, Bi^{3+}, and Ba^{2+} rather than B-site Ti^{4+} [29, 44] as discussed before, which may result in the generation of some of the A-site vacancies when Bi^{3+} replaces Na^+. These vacancies can reduce ferroelectric long-range ordering and weaken the coupling between A-site ions and TiO_6 octahedron, as a result inducing the phase change at lower temperature [29, 44]. Our results agree with the literature but also reveal that the T_d can be reduced and shifted towards lower temperature not only by changing the Bi^{3+}/Na^+ ratio but also by modifying all the A-site ions (Na^+, Bi^{3+}, and Ba^{2+}) contents [2, 24, 33].

Comparing T_d values obtained by the two methods, the pyroelectric method shows T_d values slightly lower than the dielectric method, which is in agreement with the literature [32].

Effects of nonstoichiometry composition on pyroelectric properties

Modifying the stoichiometry state of the start composition can significantly affect the pyroelectric coefficient (p) of NBT–0.06BT material. However, the efficient way for evaluating the pyroelectric material performance is to calculate the figure of merits (FOMs) that represent the essential parameters for the pyroelectric applications [32]. The calculation of the FOMs is based on the values of the pyroelectric coefficient, relative dielectric permittivity, dielectric loss, and the specific heat [29]. There are several types of FOMs depending on special types of the pyroelectric applications such as infrared or thermal imaging [21, 45]. The types of FOMs depend on the input of thermal or electrical circuits, current, or voltage [8, 14, 32].

In this study, the pyroelectric coefficient (p) of NBT–0.06BT and N_xB_yT–$0.06B_zT$ was measured from 20 to 90 °C for stoichiometric Composition (A) or T_d for nonstoichiometric Compositions B, C, and D. The

calculations of the pyroelectric coefficient (p) and FOMs were carried out using Eqs. 2–6 [9, 15, 18].

$$I_p = pA\frac{dT}{dt} \tag{2}$$

$$F_i = \frac{p}{Cv} \tag{3}$$

$$F_v = \frac{p}{Cv\varepsilon_o\varepsilon_r} \tag{4}$$

$$F_D = \frac{p}{Cv\sqrt{\varepsilon_o\varepsilon_r \tan\delta}} \tag{5}$$

$$F_C = \frac{p}{\sqrt{\varepsilon_r}} \tag{6}$$

where T is absolute temperature, t is the time, p is the pyroelectric coefficient, I_p is the pyroelectric current, F_i is the high current (i) detectivity, F_v is the high voltage (v) detectivity, F_D is high the detectivity and F_C is the pyroelectric figure of merit. C_v* is the specific heat (2.8 J K^{-1} cm^{-3}, quoted from Ref. [14]), ε_r is the relative dielectric permittivity, and ε_o is the permittivity of free space.

Figure 5 shows the change of p versus T for all compositions from 20 to 90 °C, with Composition B showing the highest p value at RT. In the temperature range from 33 to 70 °C, Compositions C and D have similar pyroelectric coefficient values with a very close maximum value of p. In contrast, Composition B shows a very characteristic peak p value. Generally, pyroelectric materials show one sharp peak at a phase transition temperature as with Composition B. However, it is very evident that the broad flat profiles for Compositions C and D in the temperature range (33–70 °C) must be linked to a different compositional structure. The composition of both samples is located at the MPB. At T_d, their structure has been changed to tetragonal with antiferroelectric or relaxor state. However, with the increase in temperature, the structure and polarization states possibly changed from rhombohedral and tetragonal coexisting (MPB) ferroelectric to tetragonal ferroelectric and then to tetragonal antiferroelectric or relaxor. This phase transition may give the pyroelectric coefficient with a broad flat peak temperature region.

The p, and FOMs F_i, F_v, and F_D values for all compositions are listed in Table 2 at RT, while those values at 90 °C or T_d are listed in Table 3.

The pyroelectric coefficients of nonstoichiometric compositions vary but are higher than Composition A at RT and T_d.

Table 2 Pyroelectric coefficient (p) and FOMs (F_i, F_v, and F_D) results at RT of NBT–0.06BT and N_xB_yT–$0.06B_zT$ in the present study and literature

Composition, name	$p \times 10^{-4}$ (C m^{-2} °C^{-1}) at RT	$F_i \times 10^{-10}$ (m.V^{-1}) at RT	F_v (m^2 C^{-1}) at 1 kHz at RT	$F_D \times 10^{-6}$ (Pa$^{-1/2}$) at 1 kHz at RT	References
NBT–0.06BT, A	3.14	1.12	0.021	9.08	This study
$N_{0.52}B_{0.52}T$–0.06BT, B	6.99	2.50	0.047	16.63	This study
$N_{0.5}B_{0.534}T$–0.06BT, C	4.77	1.71	0.022	8.32	This study
$N_{0.5}B_{0.534}T$–$0.06B_{1.02}T$, D	4.20	1.50	0.018	6.96	This study
PZT	4.14	1.42	0.008	9.01	[9, 19]
NBT–0.065BT	4.60	–	–	–	[15]
NBT–0.06BT–0.002Mn	3.51	–	–	–	[14, 30]
NBT–0.07BZT	5.73	2.03	0.022	10.52	[7, 9, 19]
BNKBT	3.25	1.95	0.026	13.43	[9, 19]
KNLNTS	1.94	0.93	0.007	11.51	[9, 19]
NKLBT–0.05BT	3.61	1.27	0.017	–	[32]

Table 3 Pyroelectric coefficient (p) and FOMs (F_i, F_v, and F_D) results at T_d of NBT–0.06BT and N_xB_yT–$0.06B_zT$ ceramics in the present study and literature

Composition, name	$p \times 10^{-4}$ (C m^{-2} °C^{-1}) at 90 °C or T_d	$F_i \times 10^{-10}$ (m V^{-1}) at 90 °C or T_d	F_v (m^2 C^{-1}) at 1 kHz at 90 °C or T_d	$F_D \times 10^{-6}$ (Pa$^{-1/2}$) at 1 kHz at 90 °C or T_d	References
NBT–0.06BT, A	23.91 at 90 °C	8.60 at 90 °C	0.19 at 90 °C	65.51 at 90 °C	This study
$N_{0.52}B_{0.52}T$–0.06BT, B	75.33 at 82.7 °C	26.92 at 82.7 °C	0.39 at 82.7 °C	138.72 at 82.7 °C	This study
$N_{0.5}B_{0.534}T$–0.06BT, C	35.24 at 60.0 °C	12.61 at 60.0 °C	0.13 at 60.0 °C	52.34 at 60.0 °C	This study
$N_{0.5}B_{0.534}T$–$0.06B_{1.02}T$, D	34.93 at 60.6 °C	12.54 at 60.6 °C	0.12 at 60.6 °C	49.80 at 60.6 °C	This study
NBT–0.07BZT	20.01 at 50 °C	7.33 at 50 °C	0.07 at 50 °C	33.62 at 50 °C	[9, 19]
NBT–0.07BZT	22.10 at 87 °C	–	–	–	[9, 19]

Table 4 The figure of merit F_C, results at room temperature and at 100 and 1000 (Hz) of NBT–0.06BT and N_xB_yT–$0.06B_zT$ ceramics

Composition, name	FOM, F_C ($\times 10^{-9}$ C cm^{-2} °C^{-1}) at RT	
	100 Hz	1000 Hz
NBT–0.06BT, A	1.53	1.58
$N_{0.52}B_{0.52}T$–0.06BT, B	2.58	2.86
$N_{0.5}B_{0.534}T$–0.06BT, C	1.52	1.60
$N_{0.5}B_{0.534}T$–$0.06B_{1.02}T$, D	1.31	1.37

Composition B shows the optimum p value at both RT and T_d (Tables 2 and 3). This may be linked to the microstructural change due to the change of the stoichiometric state of this composition. Composition B has a bigger c/a ratio than all other compositions (Table 1), indicating that Composition B has more tetragonality in its structure than all other compositions [13, 43, 44, 46, 47]. Importantly, at RT, the p values for nonstoichiometry compositions are higher than that of PZT and other lead-free compositions (Table 2) [7, 19, 27, 32].

The F_i, F_v, and F_D show also an increasing trend as p at RT. Compared with PZT and other lead-free compositions (Table 2) [7, 9, 29, 30, 42], the nonstoichiometry compositions have higher F_i, F_v, and F_D values at RT with Composition B showing the highest value at RT and T_d (Tables 2 and 3) from this study. The optimum F_v and F_D values (Tables 2 and 3) were observed for Composition B at both RT and T_d, which can be linked to the lower ε_r and the higher p values observed at these temperatures compared to Compositions C and D. Also the stoichiometry

composition A has a better F_D value than C and D due mainly to the increases in ε_r and tanδ in this nonstoichiometry compositions.

The F_C values of stoichiometry and nonstoichiometry compositions at RT and at two frequencies 100 and 1000 (Hz) were calculated (Table 4). The F_C values revealed a strong dependence upon x, y, and z contents. Generally, the materials suitable for infrared detectors should have a F_C threshold value $\sim 3 \pm 1 \times 10^{-9}$ C cm^{-2} °C^{-1} [15]. Composition B shows F_C values which are within the threshold range. Compositions A, C, and D present lower and close to that the RodrÍguez-Ruiz et al. [15] founded for a $0.935Na_{0.5}Bi_{0.5}TiO_3$–$0.065BaTiO_3$ composition which is around 1.44×10^{-9} C cm^{-2} °C^{-1}. Thus, the composition of Composition B is a promising candidate for this particular pyroelectric application.

Conclusion

The stoichiometry NBT–0.06BT and nonstoichiometry N_xB_yT–$0.06B_zT$ ceramic compositions were prepared by a conventional solid-state technique. The pyroelectric properties of these compositions were investigated, and their values were better than those in PZT and other lead-free ceramic compositions.

XRD indicates that all compositions phase structures are at the MPB region. The lattice parameter values and c/a ratio slightly change in nonstoichiometry compositions. The average grain size reduces from 1.79 (A) to 1.41 µm (D). Moreover, the stoichiometry composition shows a higher density than the nonstoichiometry compositions. Both relative permittivity (ε_r) and dielectric loss (tanδ) are affected by change in the stoichiometric state of the compositions and show an increase with the increase in x, y, and z contents.

The T_d was subjectively identified by two different methods and decreases from ~ 115 °C in Composition A to around 55 °C in Composition C, as predicted by the dielectric method. However, the T_d value for Composition C was ~ 60 °C according to pyroelectric coefficient method which questions the accuracy of the two techniques to give a definitive answer. However, it was evident that certain compositions showed much clearer maxima to pinpoint the T_d, compared to others, which suggests that the techniques may still be valid.

Composition B has the optimum p at RT and T_d. The F_i, F_v, and F_D increase with the increase in Na$^+$ (x) and Bi^{3+} (y) contents up to $x = y = 0.52$ at both RT and T_d. The F_C shows the optimum values in Composition B. The results presented in this study demonstrate that the nonstoichiometry $N_{0.52}B_{0.52}T$–0.06BT composition is a promising material for infrared detectors and other pyroelectric applications in a wide range of temperatures and frequencies.

Compliance with ethical standards

Conflict of interest We declare that we have no conflict of interest because there is no funding received for this work.

Open Access

This article is distributed under the terms of the Creative Commons Attribution 4.0 International License (http://creativecommons.org/licenses/by/4.0/), which permits unrestricted use, distribution, and reproduction in any medium, provided you give appropriate credit to the original author(s) and the source, provide a link to the Creative Commons license, and indicate if changes were made.

References

[1] García JE (2016) Elastic, dielectric and electromechanical properties of $(Bi_{0.5}Na_{0.5})TiO_3$–$BaTiO_3$ piezoceramics at the morphotropic phase boundary region. J Alloys Compd. doi:10.1016/j.jallcom.2016.08.116

[2] Balakt AM, Shaw CP, Zhang Q (2016) The effects of Ba^{2+} content on depolarization temperature and pyroelectric properties of lead-free $0.94Na_{0.5}Bi_{0.5}TiO_3$–0.06Ba1 + xTiO$_3$ ceramics. J Mater Sci Mater Electron 27:12947–12954. doi:10.1007/s10854-016-5433-1

[3] Jo W, Schaab S, Sapper E et al (2011) On the phase identity and its thermal evolution of lead free $(Bi_{1/2}Na_{1/2})TiO_3$–6 mol BaTiO$_3$. J Appl Phys. doi:10.1063/1.3645054

[4] Ma C, Tan X (2010) Phase diagram of unpoled lead-free ceramics. Solid State Commun 150:1497–1500. doi:10.1016/j.ssc.2010.06.006

[5] McQuade RR, Dolgos MR (2015) A review of the structure-property relationships in lead-free piezoelectric $(1 − x)Na_{0.5}Bi_{0.5}TiO_3$–$(x)BaTiO_3$. J Solid State Chem 3:1–8. doi:10.1016/j.jssc.2016.01.008

[6] Cheng SY, Shieh J, Lu HY et al (2013) Structure analysis of bismuth sodium titanate-based A-site relaxor ferroelectrics by electron diffraction. J Eur Ceram Soc 33:2141–2153. doi:10.1016/j.jeurceramsoc.2013.03.020

[7] Guo F, Yang B, Zhang S et al (2013) Enhanced pyroelectric property in $(1 - x)(Bi_{0.5}Na_{0.5})TiO_3–xBa(Zr_{0.055}Ti_{0.945})O_3$: role of morphotropic phase boundary and ferroelectric-anti-ferroelectric phase transition. Appl Phys Lett 103:182906. doi:10.1063/1.4828675

[8] Lau ST, Cheng CH, Choy SH et al (2008) Lead-free ceramics for pyroelectric applications. J Appl Phys 103:10–13. doi:10.1063/1.2927252

[9] Martínez FL, Hinojosa J, Doménech G et al (2013) Dielectric constant tunability at microwave frequencies and pyroelectric behavior. IEEE Trans Ultrason Ferroelectr Freq Control 60:1595–1602. doi:10.1109/TUFFC.2013.2740

[10] Razak KA, Yip CJ, Sreekantan S (2011) Synthesis of $(Bi_{0.5}Na_{0.5})TiO_3$ (BNT) and Pr doped BNT using the soft combustion technique and its properties. J Alloys Compd 509:2936–2941. doi:10.1016/j.jallcom.2010.11.163

[11] Chen M, Xu Q, Kim BH et al (2008) Structure and electrical properties of $(Na_{0.5}Bi_{0.5})1 - xBa_xTiO_3$ piezoelectric ceramics. J Eur Ceram Soc 28:843–849. doi:10.1016/j.jeurceramsoc.2007.08.007

[12] Kanuru SR, Baskar K, Dhanasekaran R (2016) Synthesis, structural, morphological and electrical properties of NBT–BT ceramics for piezoelectric applications. Ceram Int 42:6054–6064. doi:10.1016/j.ceramint.2015.12.162

[13] Jo W, Daniels J, Damjanovic D et al (2013) Two-stage processes of electrically induced-ferroelectric to relaxor transition in $0.94(Bi_{1/2}Na_{1/2})TiO_3–0.06BaTiO_3$. Appl Phys Lett 102:192903. doi:10.1063/1.4805360

[14] Abo J, Kobune M, Nishimura T, Yazaw T, Nakai Y (2006) Effects of manganese addition on pyroelectric properties of $(Bi_{0.5}Na_{0.5}TiO_3)$ 0.94 $(BaTiO_3)$ 0.06 ceramics. Integr Ferroelectr 80:87–95. doi:10.1080/10584580600656502

[15] Rodríguez-Ruiz R, González-Ballesteros R, Flores-Cuautle A, Suaste-Gómez E (2008) Determination of the pyroelectric coefficient for $(Bi_{0.5}Na_{0.5})0.935$ Ba0.065 TiO_3 piezoelectric ceramics. Ferroelectrics 368:216–223. doi:10.1080/00150190802368537

[16] Balakt AM, Shaw CP, Zhang Q (2016) The decrease of depolarization temperature and the improvement of pyroelectric properties by doping Ta in lead-free $0.94Na_{0.5}Bi_{0.5}TiO_3–0.06BaTiO_3$ ceramics. Ceram Int. doi:10.1016/j.ceramint.2016.12.004

[17] Balakt AM, Shaw CP, Zhang Q (2016) Enhancement of pyroelectric properties of lead-free $0.94Na_{0.5}Bi_{0.5}TiO_3–0.06BaTiO_3$ ceramics by La doping. J Eur Ceram Soc. doi:10.1016/j.jeurceramsoc.2016.12.021

[18] Byer RL, Roundy CB (1972) Pyroelectric coefficient direct measurement technique and application to a nsec response time detector. IEEE Trans Sonics Ultrason 19:333–338. doi:10.1109/T-SU.1972.29679

[19] Xu C, Lin D, Kwok KW (2008) Structure, electrical properties and depolarization temperature of $(Bi_{0.5}Na_{0.5})TiO_3–BaTiO_3$ lead-free piezoelectric ceramics. Solid State Sci 10:934–940. doi:10.1016/j.solidstatesciences.2007.11.003

[20] Rawat M, Yadav KL, Kumar A et al (2012) Structural, dielectric and conductivity properties of Ba^{2+} doped $(Bi_{0}0.5)TiO_3$ ceramic. Adv Mater Lett 3:286–292. doi:10.5185/amlett.2012.2322

[21] Li Q, Wang J, Ma L et al (2016) Large electrocaloric effect in $(Bi_{0.5}Na_{0.5})0.94Ba0.06TiO_3$ lead-free ferroelectric ceramics by La_2O_3 addition. Mater Res Bull 74:57–61. doi:10.1016/j.materresbull.2015.10.010

[22] Search H, Journals C, Contact A, Iopscience M (1991) $(Bi_{1/2}Na_{1/2})$ $TiO_3–BaTiO_3$ system for lead-free piezoelectric ceramics. Jpn J Appl Phys 2236:2236–2239

[23] Shannon RD (1976) Revised effective ionic radii and systematic studies of interatomic distances in halides and chalcogenides. Acta Crystallogr Sect A 32:751–767. doi:10.1107/S0567739476001551

[24] Li M, Zhang H, Cook SN et al (2015) Dramatic influence of A-site nonstoichiometry on the electrical conductivity and conduction mechanisms in the perovskite oxide $Na_{0.5}Bi_{0.5}TiO_3$. Chem Mater 27:629–634. doi:10.1021/cm504475k

[25] Hiruma Y, Nagata H, Takenaka T (2009) Formation of morphotropic phase boundary and electrical properties of $(Bi_{1/2}Na_{1/2})TiO_3–Ba(Al_{1/2}Nb_{1/2})O_3$ solid solution ceramics. Jpn J Appl Phys 48:09KC08. doi:10.1143/JJAP.48.09KC08

[26] Kumari R, Ahlawat N, Agarwal A et al (2016) Structural transformation and investigation of dielectric properties of Ca substituted $(Na_{0.5}Bi_{0.5})0.95 - xBa_{0.05}Ca_xTiO_3$ ceramics. J Alloys Compd. doi:10.1016/j.jallcom.2016.11.200

[27] Cho J-H, Jeong Y-H, Nam J-H et al (2014) Phase transition and piezoelectric properties of lead-free $(Bi_{1/2}Na_{1/2})TiO_3–BaTiO_3$ ceramics. Ceram Int 40:8419–8425. doi:10.1016/j.ceramint.2014.01.051

[28] Le Goupil F, Bennett J, Axelsson AK et al (2015) Electrocaloric enhancement near the morphotropic phase boundary in lead-free NBT–KBT ceramics. Appl Phys Lett 107:103–107. doi:10.1063/1.4934759

[29] Yoon MS, Khansur NH, Ur SC (2010) The effect of pre-milling/pre-synthesis process and excess Ba on the microstructure and dielectric/piezoelectric properties of nano-sized $0.94[(Bi_{0.5}Na_{0.5})TiO_3]–0.06[Ba(1 + x)TiO_3]$. Ceram Int 36:1265–1275. doi:10.1016/j.ceramint.2010.01.011

[30] Hiruma Y, Yoshii K, Nagata H, Takenaka T (2007) Investigation of phase transition temperatures on $(Bi_{1/2}Na_{1/}$

$_2$)TiO$_3$–(Bi$_{1/2}$K$_{1/2}$)TiO$_3$ and (Bi$_{1/2}$Na$_{1/2}$)TiO$_3$–BaTiO$_3$ lead-free piezoelectric ceramics by electrical measurements. Ferroelectrics 346:114–119. doi:10.1080/00150190601180471

[31] Guggilla P, Batra AK, Currie JR et al (2006) Pyroelectric ceramics for infrared detection applications. Mater Lett 60:1937–1942. doi:10.1016/j.matlet.2005.05.086

[32] Anton EM, Jo W, Damjanovic D, Rdel J (2011) Determination of depolarization temperature of (Bi$_{1/2}$Na$_{1/2}$)TiO$_3$-based lead-free piezoceramics. J Appl Phys 110:1–14. doi:10.1063/1.3660253

[33] Guo Y, Gu M, Luo H (2011) Antiferroelectric phase and pyroelectric response in (Na$_y$Bi$_z$)Ti1 − xO$_3$(1 − x)–xBaTi$_3$ ceramics. J Am Ceram Soc 94:1350–1353. doi:10.1111/j.1551-2916.2011.04509.x

[34] Sapper E, Schaab S, Jo W et al (2012) Influence of electric fields on the depolarization temperature of Mn-doped (1 − x)Bi$_{1/2}$Na$_{1/2}$TiO$_3$–xBaTiO$_3$. J Appl Phys 111:14105. doi:10.1063/1.3674275

[35] Levanyuk AP (2015) Phase transitions and domain structures in thin ferroelectric films. Phase Transit 88:682–691. doi:10.1080/01411594.2014.986732

[36] Lichtensteiger C, Fernandez-Pena S, Weymann C et al (2014) Tuning of the depolarization field and nanodomain structure in ferroelectric thin films. Nano Lett 14:4205–4211. doi:10.1021/nl404734z

[37] Okatan MB, Mantese JV, Alpay SP (2010) Effect of space charge on the polarization hysteresis characteristics of monolithic and compositionally graded ferroelectrics. Acta Mater 58:39–48. doi:10.1016/j.actamat.2009.08.055

[38] Ranjan R, Dviwedi A (2005) Structure and dielectric properties of (Na$_{0.50}$Bi$_{0.50}$)1 − xBaxTiO$_3$: 0 ≤ x ≤ 0.10. Solid State Commun 135:394–399. doi:10.1016/j.ssc.2005.03.053

[39] Zhang S, Kounga AB, Aulbach E et al (2008) Lead-free piezoceramics with giant strain in the system Bi$_{0.5}$Na$_{0.5}$TiO$_3$–BaTiO$_3$–K$_{0.5}$Na$_{0.5}$NbO$_3$. II. Temperature dependent properties. J Appl Phys 103:34108. doi:10.1063/1.2838476

[40] Anem S, Rao KS, Rao KH (2016) Investigation of lanthanum substitution in lead-free BNBT ceramics for transducer applications. Ceram Int. doi:10.1016/j.ceramint.2016.06.173

[41] Kang W-S, Lee S-K, Koh J-H (2015) AC conductivity and dielectric properties of (Bi, Na)TiO$_3$–BaTiO$_3$ lead free ceramics. Ceram Int 41:6925–6932. doi:10.1016/j.ceramint.2015.01.147

[42] Wang X, Tang X, Chan H (2004) Electromechanical and ferroelectric properties of (Bi$_{1/2}$Na$_{1/2}$)TiO$_3$–(Bi$_{1/2}$K$_{1/2}$)TiO$_3$–BaTiO$_3$ lead-free piezoelectric ceramics. Appl Phys Lett 85:91. doi:10.1063/1.1767592

[43] Yao Z, Chu R, Xu Z et al (2016) Processing and enhanced electrical properties of Sr1 − x(K$_{0.5}$Bi$_{0.5}$)xBi$_2$Nb$_2$O$_9$ lead-free piezoelectric ceramics. Ceram Int 42:10619–10623. doi:10.1016/j.ceramint.2016.03.156

[44] Li XJ, Xi ZZ, Long W, Fang PY (2013) Synthesis of antiferroelectric (Bi$_{0.5}$34Na$_{0.5}$)0.94Ba0.06TiO$_3$ ceramics with high phase transition temperature and broad temperature range by a solid-state reaction method. Chin Sci Bull 58:2893–2897. doi:10.1007/s11434-013-5972-2

[45] Xu Q, Huang DP, Chen M et al (2009) Effect of bismuth excess on ferroelectric and piezoelectric properties of a (Na$_{0.5}$Bi$_{0.5}$)TiO$_3$–BaTiO$_3$ composition near the morphotropic phase boundary. J Alloys Compd 471:310–316. doi:10.1016/j.jallcom.2008.03.078

[46] Craciun F, Galassi C, Birjega R (2012) Electric-field-induced and spontaneous relaxor-ferroelectric phase transitions in (Na$_{1/2}$Bi$_{1/2}$)1 − XBa xTiO$_3$. J Appl Phys. doi:10.1063/1.4770326

[47] Patel S, Chauhan A, Kundu S et al (2015) Tuning of dielectric, pyroelectric and ferroelectric properties of 0.715Bi$_{0.5}$Na$_{0.5}$TiO$_3$–0.065BaTiO$_3$–0.22SrTiO$_3$ ceramic by internal clamping. AIP Adv 5:87145. doi:10.1063/1.4929328